

# Wing positioning

Using FloWizard CFD to optimise a wing's location on a simplified Touring Car model revealed some surprisingly complicated interactions

**W**hat effect does the position of a rear wing on a racecar have on its performance?

The relationship between the two is known to be critical, but where do you start? Sadly, there seems to be an almost complete lack of information in print that can be readily applied in the real world, so when the opportunity to take a close look at a practical case presented itself we decided to share some of the general

BY SIMON MCBEATH

insights that arose. Hopefully, the findings will help readers with their own installations.

## PREFERRED POSITION

The available literature on this subject provides few references on this wing/body relationship. Joseph Katz helps in *Race Car Aerodynamics* by quoting an SAE paper (920349) in which wing heights between 0.5 and 5.5 times the wing chord above

the rear deck were evaluated on generic Sports Prototype and sedan racecars. But in most competition categories wing height is likely to be less than a single wing chord dimension, so this reference only provided a couple of practically useful data points, and in both cases the published graphs showed this to be perhaps the most crucial part of the data set. And as a single wing angle only was cited in each case, more examples at and below a single chord above

the rear deck, and at a range of angles, would be invaluable.

So when *Racecar Engineering* contributor Marshall Pruett's Motorsport Engineering (MPME) requested assistance in mapping the mandatory wing profile used in the SCCA's Speed World Challenge Touring Car division, in which the team competes with Scion tC racecars, it was agreed that it would be best if the actual environment in which the wing was to work could be simulated. With little time and only modest

## MODELLING PROFILES

Figure 1

CAD model of the mandatory single-element wing used in SCCA Touring Cars



Figure 2

Graph showing downforce and drag forces calculated by FloWizard for the wing in isolation

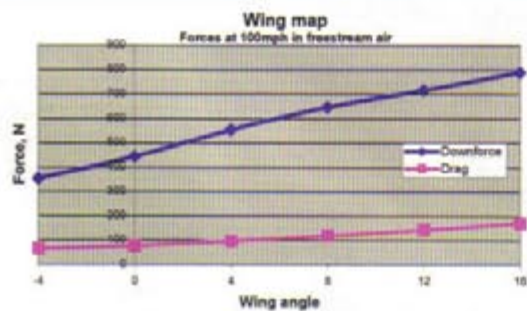


Figure 3

CAD model of the simplified car



Figure 4

Flow vectors along the wingless car centreline

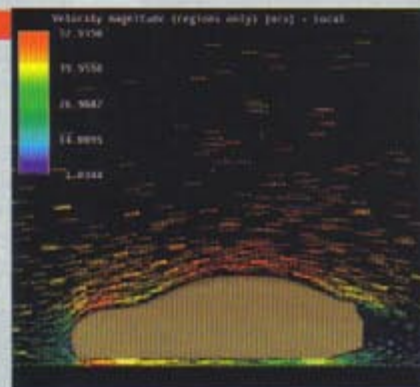
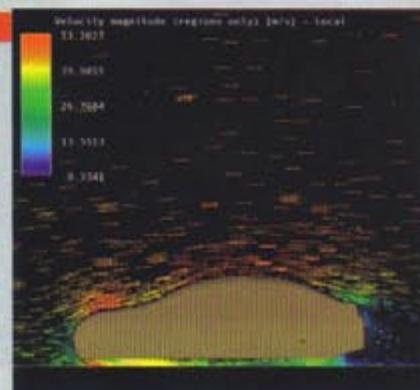


Figure 5

Flow vectors along the wingless car 0.6m out from the centreline



computing resources available, it was decided to generate a very simple 3D CAD model that incorporated the basic side view and front view profiles of the car, these profiles being derived from photos on the manufacturer's website. The hope was that using the essential features of the body shape would provide a more realistic environment for the wing to operate in, and that this would then allow some trends as to the best height and angle for the wing to be obtained. The study performed was therefore in similar spirit to those performed on other simplified reference bodies that appear in various aerodynamic texts.

The regulations for the series not only mandate a specific wing profile, they also specify a maximum height for any part of the wing at six inches (150mm) below the maximum roof height, and a maximum rearward location no further back than the rear of the approved bodywork. These locations are here designated h-max for the maximum height and x-max for the rearward position. It was decided to use x-max locations only, that is all positions

to be tested would feature the wing as far back on the car as the rules permitted. And that four wing heights would be tested, each at a range of wing angles. Chosen heights were: the maximum permitted; h-max, which was set at 150mm below maximum roof height (with the wing horizontal this meant the leading edge was roughly one chord dimension above the rear deck); and three additional lower heights at h-max-30mm, -60mm and -90mm. In each case, as the wing was rotated, its position was reset so that the highest point of the end plate matched these figures, and that the rearmost point of the end plate met the maximum rearward location rule.

#### INITIAL MODELS AND RUNS

The first task was to produce the wing to the mandatory profile. A scanned outline drawing of the profile was carefully measured to generate a set of points through which a spline curve could be fitted in the CAD software. The 2D profile was then scaled to the

correct chord dimension (215mm, or approx 8.5in) and then extruded in 3D to the maximum allowed span (1.22m, including a pair of simple end plates, or roughly 48in). The wing model is shown in figure 1, and the map of downforce and drag forces obtained using default FlowWizard settings at 100mph (44.7m/s) is shown in figure 2.

Next, the CAD model of the car had to be tested in the CFD software. The auto meshing

**all positions tested would feature the wing as far back on the car as rules permitted**

facility of FlowWizard is unable to deal with volumes between 'solid' objects that taper away to nothing, such as the intersection of cylinders representing tyres with the flat plane representing the ground. So, as much for speed in generating the model as to enable the automatic meshing to take place, the wheels were simply constructed as quadrilateral block shapes to

approximate the correct overall dimensions. This gave four contact patches that would not only mesh, but which would also enable the car model to be attached to the ground plane in FlowWizard and enable runs at a representative ground clearance - a significant factor in obtaining realistic flows over the top of the car.

The car model was subjected to CFD and is shown in figure 3 while figures 4 to 9 show various

post-processed CFD-generated graphics illustrating the flows around the wingless car. Total lift and drag were calculated

on the car model as 572.7N (128.4lb) and 1113.5N (249.7lb) respectively, corresponding to a lift coefficient of +0.248 and a drag coefficient of 0.482. While not representative of the real car, the changes to these numbers brought about by the wing could at least be assessed.

Looking at the area over the rear screen and deck where the rear wing operates, it would

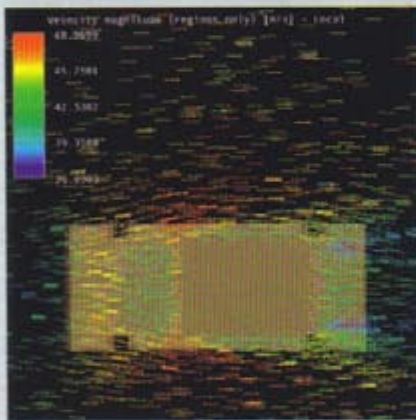


**Figure 6**  
Flow vectors along the wingless car from above at h-max, 150mm below the roof peak

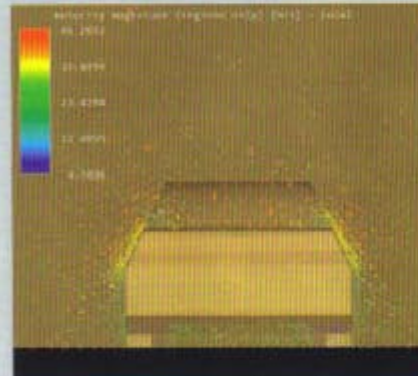


**Figure 8**  
Flow vectors across the wingless car from behind on a plane just ahead of where the wing leading edge would be

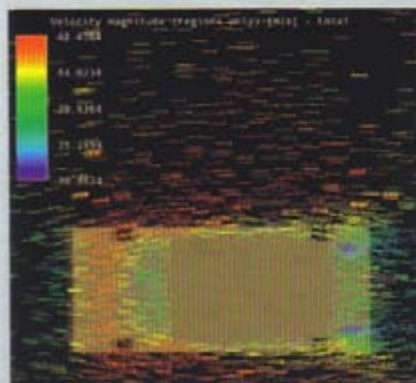


**Figure 7**  
Flow vectors along the wingless car from above at h-max -90mm, 240mm below the roof peak

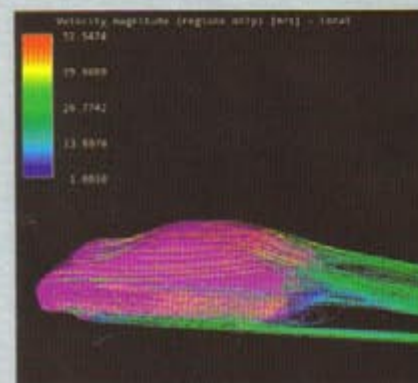


**Figure 9**  
Path lines demonstrate the complexity of the flow field around this generic Touring Car

LIFT OVER DRAG

Figure 10

Total lift on the car plus wing, with the wing at its maximum permitted height

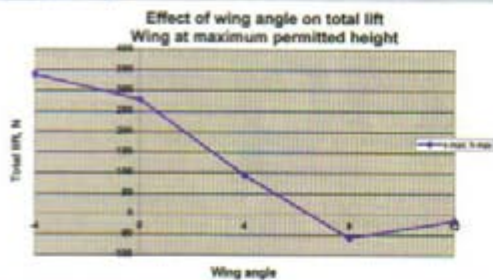


Figure 11

The car's total drag with the wing at maximum height

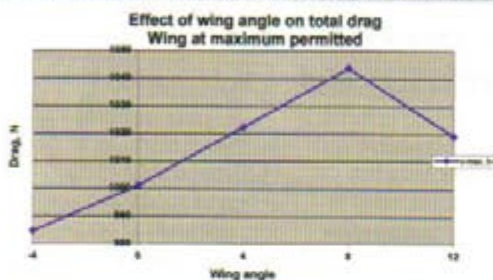


Figure 12

Lift over drag, calculated using changes to the coefficients relative to the no-wing case

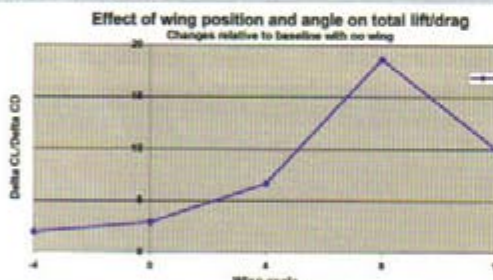


Figure 13

The downforce generated by the wing alone at h-max

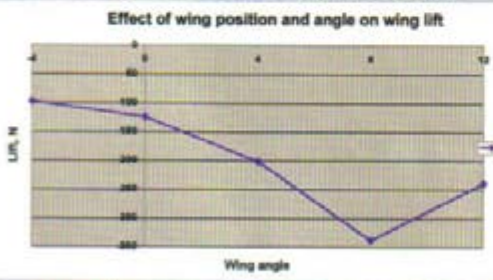
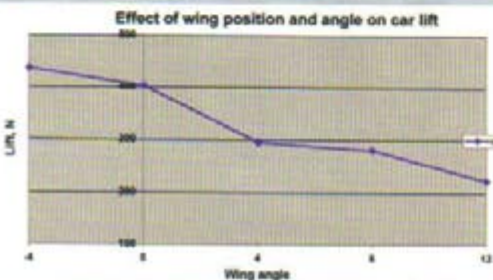


Figure 14

The lift on the car only as the wing angle is adjusted at h-max



appear that the general character of the flow field has been captured using this simple model and CFD parameters. Clearly the flow over much of the rear screen has a pronounced downward direction to it (figure 4, centreline flow vectors), and is also generally convergent around the rear (figures 6 and 7 from above), as well as spiraling in from the sides around the rear screen pillars (figure 8). Notice too though that the flow above the rear deck in figure 5, half a wing span out from the centreline, is more horizontal than it is on the centreline, so the outer portions of our 1.22m plain span wing will obviously see a different onset flow angle to the more central portions. Clearly too, air in which the wing will operate will be at varying velocities.

WING-ON-CAR TRIALS

The next step was to test the wing on the car at various heights and angles. The angle sweep on the wing in isolation showed it would run to 16 degrees without stalling. However, it seemed unlikely that it would reach this angle when over much of its span the onset flow would be approaching downwards at about 20 degrees. So the wing was mapped first at the maximum permitted height, starting with an angle of minus four degrees and continuing until performance dropped off. Figure 10 and 11 plot the total lift and drag of the car and wing combination at wing angles of up to 12 degrees, where it became apparent the wing had stalled.

Notice that even though it is partly masked by the car ahead of it, the wing is still capable of reversing the 'natural' positive lift and even turning it into a small amount of downforce at the two steepest angles run here. Consider that the eradication of lift alone would be worth about an extra six per cent vertical force on the tyres at 100mph if the car weighed 1000kg (2200lb). In this exercise we were not attempting to determine the front to rear division of the vertical aerodynamic forces, and note too that the racing version of the Scion uses a front splitter to develop front-end downforce to balance the rear wing.

Another interesting observation is that total drag appears to have been reduced by the wing at all angles, compared to the no-wing case. What appears to be happening here is that the wing lifted the general angle of flow along the back of the car and reduced its velocity over the rear screen. This further lowered the static pressure here and, because the sloping screen is partially rear-facing, reduced drag. Suddenly it opens up the idea of different configurations for different tracks, although the best setting for maximum downforce and efficiency is eight degrees at this wing height according to figure 12, which plots the ratio of the two coefficients as a measure of efficiency.

CFD software can also calculate the forces on the separate components, and figure 13 shows how much less peak downforce it is able to generate when mounted behind the car's 'greenhouse'. In fact the wing generated just 43 per cent of the freestream peak and 52 per cent of the freestream value at eight degrees. Especially interesting though is the plot in figure 14, which shows the car's lift reduces as the wing angle is increased, even after the wing's own contribution has declined at 12 degrees. To see how the wing turns the flow at the rear, take a close look at the CFD graphics in figures 15 to 17 run at the peak downforce and efficiency setting of h-max and eight degrees.

OTHER WING HEIGHTS

All the results from the first wing height seemed logical and easily explained. As additional wing heights were mapped however, the picture became much more complex. In an attempt to present the findings reasonably clearly, let's first look at the downforce generated by just the wing at the different heights above the deck, shown in figure 18. At angles of four degrees and above the wing generated less downforce in the lower positions, which we might reasonably have predicted because the wing was being moved into less energetic airflow.

However, at the shallower wing angles the pattern becomes more difficult to



explain. At all heights the wing produces less downforce than at steeper angles, but the highest downforce at zero degrees is now generated when the wing is 30mm below the maximum height. And CFD visualisations did show lower static pressure on the wing's underside at this height and angle compared to positions h-max or h-max-60mm. This appeared to be a genuine interactive effect, then, that saw the wing working harder. Things become more complex again when the wing is lowered to h-max-90mm and at an angle of minus four degrees. Interactions seem to be even more complex, but again the static pressure was lower on the wing's underside. However, there were also

different interactions with the car, and figure 19 plots the total lift of wing plus car for all the wing locations and angles tested. Here the dark blue line represents the car's total downforce with the wing at maximum height and it seems to

cases are very similar at both four and eight-degree angles, which might indicate that loss of wing downforce from reducing the height is offset by better interaction with the car. Then, at zero degrees, the wing's better performance at the -30mm

figures of the test. So another graph is needed to throw more light on this, and figure 20 shows the lift on the car body only. Here it can be seen that car body lift decreases as the wing angle increases, even when the wing has stalled at 12 degrees. Trying to define which wing height has the most effect is hard, but certainly at shallower wing angles, the lowest wing position seems to have a more pronounced effect on the body lift. And this is predominantly what gives the low net lift for the whole car seen in figure 19, although the wing itself also performed strongly at the -90mm and minus four degrees setting compared to the other heights at this angle. Static pressure is

**total drag appears to have been reduced by the wing at all angles**

follow the same pattern as the downforce of the wing only in figure 18. However, in the other instances there is clearly much more going on than just the wing's downforce altering with height. The -30mm and -60mm

height produces less overall downforce lift than either h-max or h-max-60mm. Even more curiously, at the -90mm height and minus four degree angle, the wing produced one of the best downforce

FLOW CHANGES

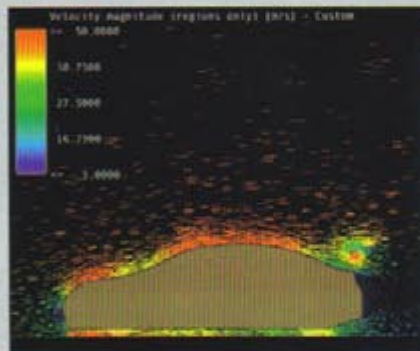


**Figure 15**  
Flow vectors along the car centreline with the wing at h-max and eight degrees

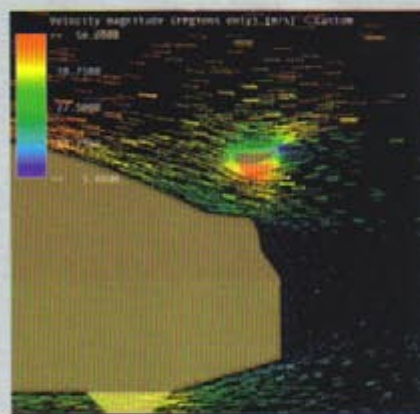


**Figure 16**  
Flow vectors along the car centreline with the wing at h-max and eight degrees

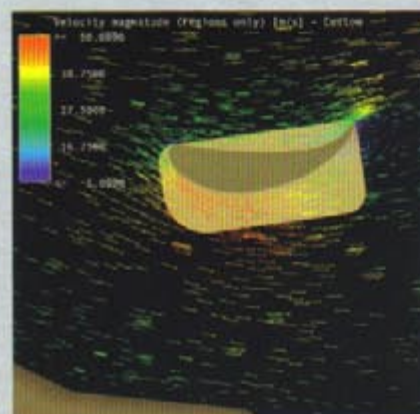
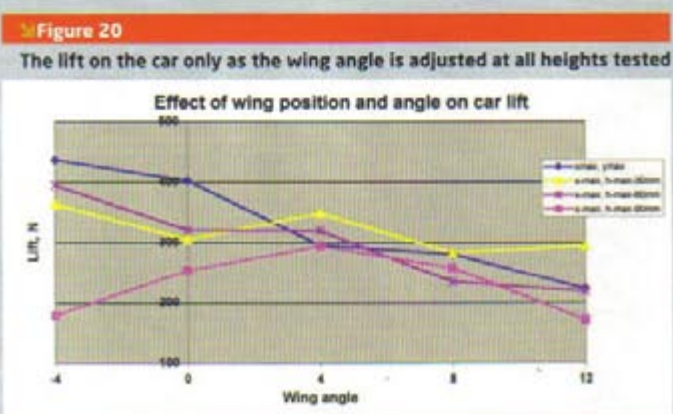
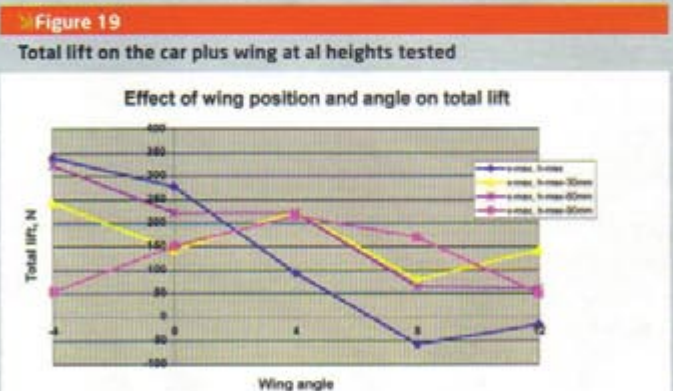
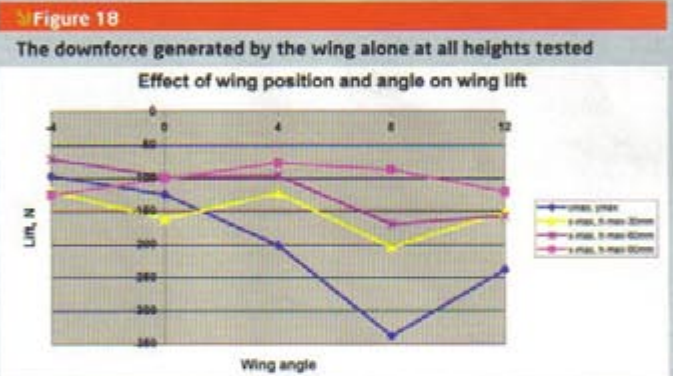


**Figure 17**  
Flow vectors along the car centreline with the wing at h-max and eight degrees



lower on the underside of the wing at -90mm and minus four degrees than it is at h-max at the same angle according to figures 21 and 22. But figures 23 and 24 show that with the wing at minus four degrees, lower pressures exist along the underbody in the lowest wing position compared to the highest, especially at the transition into the small diffuser-like ramp on this model. So there seems to be a strong interaction between the wing and the body with some combinations of wing height and angle.

## CONCLUSIONS


The final plot in figure 26 again plots the difference in lift/drag ratios for the wing positions

compared to that of the wingless car. This is a handy comparison of overall efficiency for all the wing height and angle combinations. And if there is a generalisation here it is that overall aerodynamic performance increased with wing angle. However, as to which height is optimum, this depends on the wing angle and, in all probability, on the shapes of the car and the wing. Clearly, in the example illustrated in figure 25 the rear deck and the wing combine to turn the air through more of an angle than would be expected from a wing at this angle in freestream air, or indeed just a bit higher above this rear deck. However, once the wing at this height had been rotated

to four degrees it was quite clearly stalling, so the interaction with the deck wasn't enough to overcome what may now have become too close a proximity to the deck for a good feed of air to pass under the wing. Significantly, the wing's leading edge gets closer to the deck as the angle is increased, while also keeping to the height specified in each case.

We have also seen evidence that some low wing angle heights serve to create stronger interaction with the underbody of the car model here. However, had this been a real production-based Touring Car with a rough underside then this interaction would likely have been less

strong. Conversely, had we been looking at a sports prototype racer with an unrestricted ground effect underbody then we might well expect such interactions to be more powerful.

Despite the simplicity of the racecar model used in this study, and the use of basic default CFD settings that together will not have simulated the finer details of real flows, there would appear to be considerable food for thought here. Further study with improved models of the Touring Car variety, and models representing other race categories would surely produce more thought-provoking data on the taxing question of optimising wing position. 

## PRESSURE PLOTS

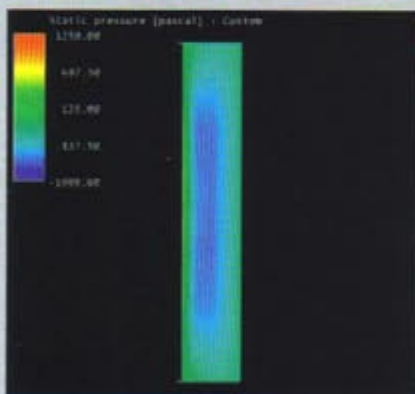


Figure 21

Static pressure on the wing underside at minus four degrees and h-max-90mm

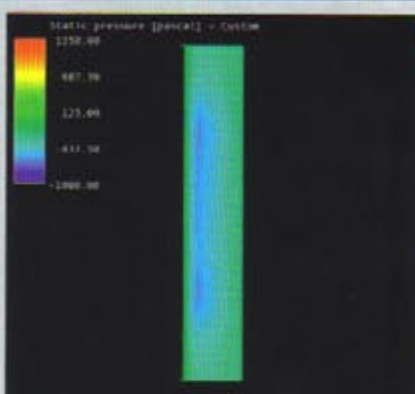


Figure 22

Static pressure on the wing underside at minus four degrees and h-max

Figure 23

Static pressure on the underbody with the wing at minus four degrees and h-max-90mm

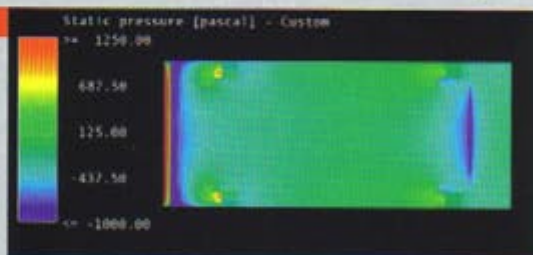


Figure 24

Static pressure on the underbody with the wing at minus four degrees and h-max

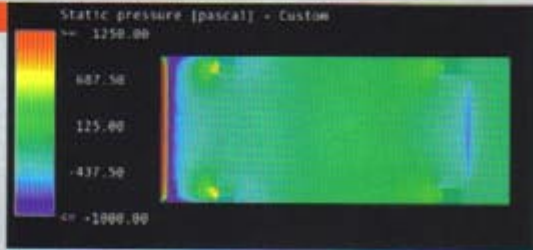


Figure 26

Lift over drag, calculated using changes to the coefficients relative to the no-wing case, for all wing heights and angles

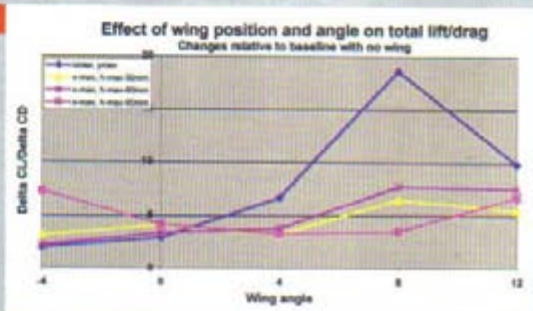
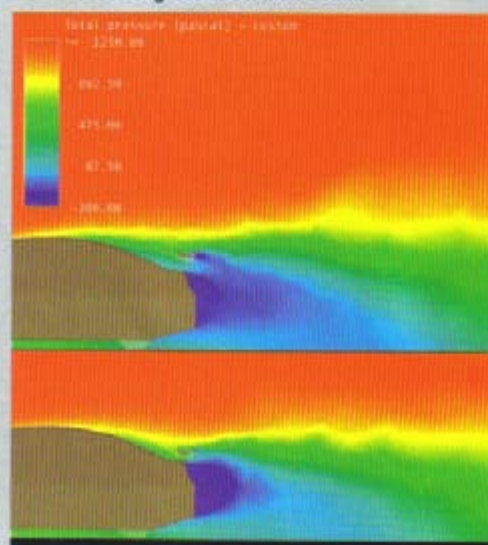


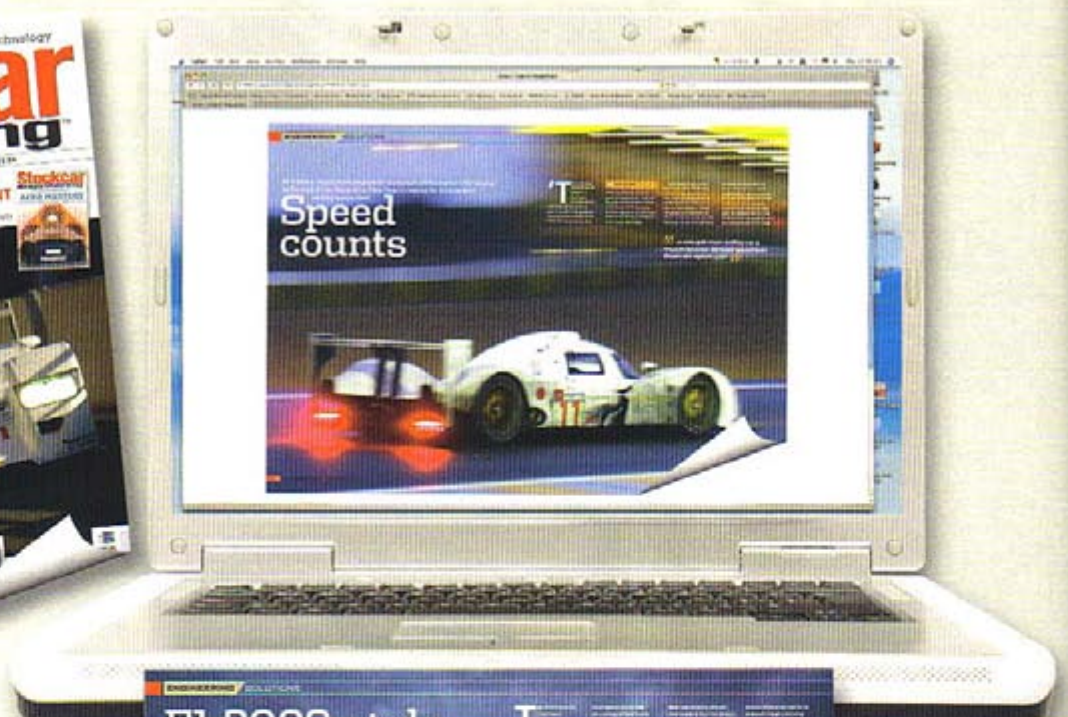
Figure 25

Total pressure plots with the wing at minus four degrees and h-max (top) compared to the wing at minus four degrees and h-max-90mm



Thanks to Ansys Europe for the use of FlowWizard 3.0.

# Get **Racecar Engineering** direct to your computer



## THE WORLD'S LEADING MOTORSPORT TECHNOLOGY PUBLICATION

Each month **Racecar Engineering** brings the best possible insight into all forms of the rapidly changing world of motorsport engineering. From keeping pace with the latest technologies to expanding your knowledge of racecar design and operation, no other magazine gets you closer



## SPECIAL OFFER

GET THREE DIGITAL ISSUES OF  
**RACECAR ENGINEERING**  
TODAY FOR JUST **£4.99/\$9.99**

Go to [www.zinio.com](http://www.zinio.com) to get a sneak preview and take up this great offer